JOURNAL OF GEOPHYSICAL RESEARCH, VOL. 103, NO. B4, PAGES 7171–7186, APRIL 10, 1998

Crustal velocity structure across the eastern Snake River Plain and the Yellowstone swell

Xiaohua Peng and Eugene D. Humphreys

Department of Geological Sciences, University of Oregon, Eugene

Abstract. Teleseismic receiver functions are used to estimate the crustal structure beneath a 36-station, 500-km-long, NW oriented linear array centered on the eastern Snake River Plain and crossing the Yellowstone hotspot swell 250 km SW of Yellowstone. Structure derived previously for this region from wide-angle reflection data is used as an initial model, and this structure explains most features observed in our receiver functions. Based on a combination of forward and inverse modeling, our data require several modifications to the initial structure: (1) Moho depth is ~42 km beneath most of the Snake River Plain, shallows to ~37 km to either side, and thickens abruptly to ~47 km beneath SW Wyoming; (2) a midcrustal layer interpreted previously as a ~9-km-thick gabbroic sill is flat topped across the entire ~90 km width of the Snake River Plain; and (3) a low-velocity layer is found beneath and southeast of the Snake River Plain, which probably is partially molten lowermost crust. Using the seismic structure of the crust to estimate the crustal load upon the mantle, and assuming local isostasy, we calculate that mantle beneath the Yellowstone swell is approximately uniformly as buoyant as 12-million-year-old ocean mantle, and more buoyant than the adjacent Wyoming mantle by an amount equivalent of ~1.5 km of elevation. The transition between these regions of greatly different mantle occurs across a major Paleozoic boundary that now separates the Basin and Range from the Rocky Mountains.

1. Introduction

The eastern Snake River Plain (SRP) is the magmatic track of the Yellowstone hotspot [*Morgan*, 1972; *Smith and Sbar*, 1974; *Pierce and Morgan*, 1990]. The SRP lies along the axis of the Yellowstone swell, a wake-like area of uplift, abundant seismicity and young faulting described as a tectonic parabola [*Anders et al.*, 1989] (Figure 1). The relatively low elevations of the SRP are attributed to magmatic densification of the crust [*Anders and Sleep*, 1992]. The crust modified by hotspot magmatism is Archean basement that experienced late Proterozoic continental rifting and thinning, upon which a westward-thicking sequence of Paleozoic sediments were deposited in seas adjacent to stable North America. The structural hingeline of Paleozoic downwarp lies within Idaho close to Idaho's eastern boundary [*Poole et al.*, 1992] (Figure 1) and is crossed by the SE end of our array. This hingeline later controlled the eastern limit of intense Mesozoic thrusting and crustal thickening, which was followed by a Cenozoic collapse and thinning of the continent, currently expressed by Basin and Range activity. Significant deformation east of the hingeline consists only of modest Laramide shortening; essentially no Cenozoic extension has occurred, and this crust remains relatively thick. Uplift history of this region is not well understood, but the entire region, now standing from 1.5 to 4 km above sea level, was near sea level prior to the Sevier overthrusting ~110 m.y. ago. The northern third of our array extends across the projection of a major Proterozoic shear zone and onto crust that is either Proterozoic or strongly modified in the Proterozoic [*Reed*, 1993; *Houston et al.*, 1993].

Copyright 1998 by the American Geophysical Union.

Paper number 97JB03615.
0148-0227/98/97JB-03615$09.00

The crust beneath much of our array has been characterized by wide-angle reflection and refraction studies. *Sparlin et al.* [1982] discuss results of an investigation that crossed the SRP near our linear array (Figure 1). Away from the SRP, Sparlin et al.'s four-layer off-plain structure (Figure 2) is consistent with *Willden*'s [1965] interpretation of explosion data recorded along a line extending SE from the SRP (Figure 1) to near the Utah-Wyoming-Colorado border. In traversing from the northern Utah Basin and Range to the southwestern Wyoming Rocky Mountains, *Braile et al.* [1974] find the crust to thicken abruptly to more than 40 km near the SE end of Willden's line.

Compared to crust adjacent to the SRP, SRP crust is modified significantly by young magmatism. An unusual intermediate velocity (6.5 km/s) unit, interpreted as a ~9-km-thick sill of basaltic composition, extends across the width of the SRP and rests on a midcrustal interface (Figure 2). *Chiang and Braile* [1984] modeled the data of *Sparlin et al.* [1982] and concluded that the sill-like feature is flat topped across the 45 km width illuminated by these data (Figure 2). Seismic profiles recorded along the axis of the eastern SRP indicate that approximately 3-6 km of volcanic rocks and interbedded sediment (of which the distinctive basaltic cover is only the upper few hundred meters) overlie a ~5-km-thick upper crustal layer of Paleozoic sediments [*Braile et al.*, 1982]. Below lie an upper crustal crystalline basement (6.1 km/s), the presumed sill and ~22 km of lower crust (6.8 km/s), for a total SRP crustal thickness of ~40 km.

A low-velocity zone, inferred to be partially molten lowermost crust, is found beneath the eastern SRP tapering from a thickness of ~20 km immediately SW of the Yellowstone Caldera to zero thickness near our experiment [*Priestley and Orcutt*, 1982]. No evidence for the low-velocity zone is found SW of our experiment. A poorly constrained upper mantle *Pn* velocity of 7.9 km/s is observed beneath the eastern SRP [*Braile et al.*, 1982]. Sparlin

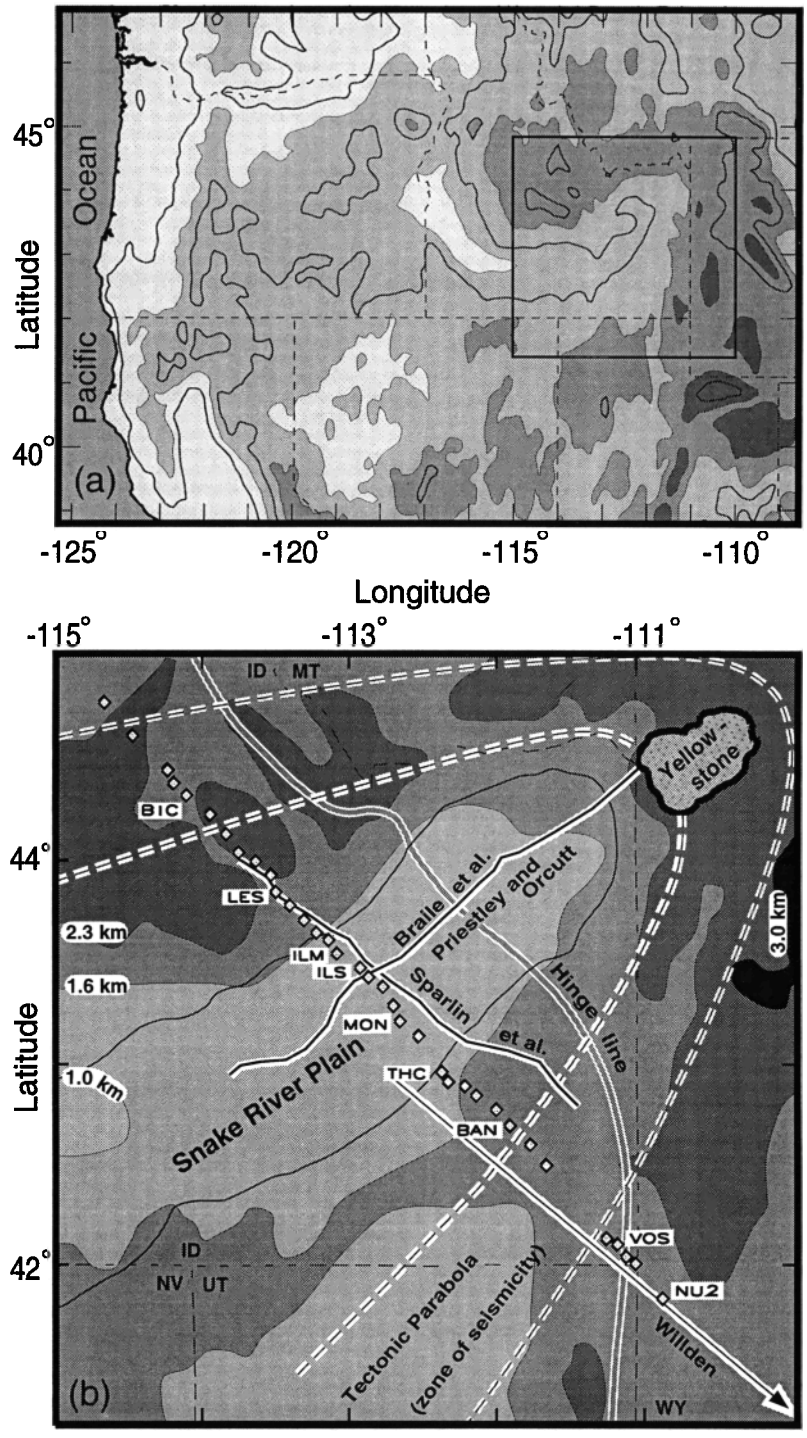

Figure 1. (a) Smoothed elevation of much of the western United States. The area in Figure 1b is shown with a box. Shading levels are in 1-km increments, and contours are shown at 0.5-km increments. (b) Smoothed elevations in the Yellowstone-eastern Snake River Plain region, including portions of Idaho (ID), Wyoming (WY), Utah (UT), Nevada (NV), and Montana (MT). The Yellowstone-eastern Snake River Plain province is outlined with a thin solid line, and the Yellowstone caldera is shown with a heavy solid line. The Paleozoic hingeline, represented by the eastern limit of Lower Cambrian terrigenous Miogeoclinal sediments [*Poole et al.*, 1992] is shown with the gray line. Dashed lines are state boundaries, and white-outlined dashed lines represent the seismically active tectonic parabola. Squares are the stations from the 1993 PASSCAL Snake River Plain experiment used in this study, with bold labeled squares indicating stations used in examples. Solid lines with white outlines indicate locations of active source seismic investigations of *Sparlin et al.* [1982], *Chiang and Braile* [1984], *Priestley and Orcutt* [1982], *Braile et al.*, [1982], and *Willden* [1965].

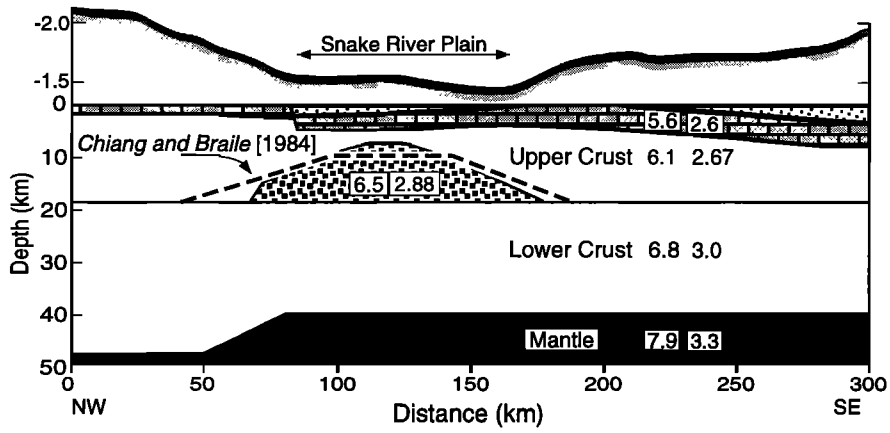

Figure 2. Crustal structure across the eastern Snake River Plain inferred by *Sparlin et al.* [1982] from seismic reflection-refraction data. Number pairs are P wave velocities in km/s (left number) and density in g/cm^3 (right number). The near-surface stipple fill represents young volcanic and sedimentary deposits with a P wave velocity of 4.5 km/s, the brick pattern represents Paleozoic sediments, and the heavy stipple pattern represents the basaltic sill. The dashed line represents the modified shape for the basaltic sill from *Chiang and Braile* [1984]. The crustal thickness increase to the NW is inferred from gravity modeling [*Sparlin et al.*, 1982]. The shaded line indicates topography (smoothed in the NE direction).

et al. infer the crust to thicken NW of the SRP (Figure 2) based on gravity data; the only seismic information on Moho depth in Sparlin et al.'s study occurs beneath the SRP. Thus, in general terms, prior study of the SRP region resolves a simple two-layer crust away from the SRP and finds that beneath the SRP this basic crust has been magmaticaly modified through the addition of specific layers.

The model that satisfies our data and requires minimal modification to the structure inferred by the earlier studies has the crust thinning to either side of the SRP, averages ~40 km in thickness across the width of the tectonic parabola, includes a lower crustal low-velocity zone beneath the SRP region (which is interpreted as partially molten lowermost crust), and has the presumed basaltic sill with a flat top at a depth of ~10 km across the ~90 km width of the SRP. Because we use the crustal velocities determined by the active source investigations, our receiver function analysis provides well-constrained estimates of crustal thickness except in regions where Moho *Ps* conversions are not observed clearly.

2. Seismic Deployment

Our investigation uses teleseismic data recorded by a Program for Array Seismic Studies of the Continental Lithosphere (PASSCAL) linear array trending SE for about 500 km from central Idaho across the SRP, the hingeline, and into SW Wyoming (Figure 1). This array was located ~250 km SW of Yellowstone and aligned perpendicular to the SRP, trending directly across the Yellowstone swell. By being oriented in line with most circum-Pacific events, this array is in plane with more than half of Earth's seismicity. Array operation occurred from May through November of 1993, using 27 broadband and 3 1-Hz, three-component seismometers. These seismometers were moved so as to occupy a total of 55 sites, providing a station spacing of about 10 km. However, the high-frequency seismometers and sites located in or near large sedimentary basins (on the SE side of the deployment) produced little data of quality usable for receiver function study, and sites located in regions of rugged topography (NW and SE of the SRP) experienced significant degradation of data quality. These problems result in array gaps, and only the 36 sites shown in Figure 1 were used in our study. About 375 teleseismic earthquakes were recorded, of which 82 were of quality suitable for use in this receiver function study. These data provided more than a thousand radial receiver functions (and an equal number of tangential receiver functions). Data quality varied greatly from one station to another and from one event to another, and about 350 receiver functions are of a quality that permit modeling of crustal structure.

3. Receiver Functions

Receiver functions commonly are used to address layered Earth structure through use of the S conversions that arrive shortly after the arrival of teleseismic P waves [*Langston*, 1977, 1979; *Burdick and Langston*, 1977; *Ammon*, 1991]. The magnitude and delay of these P-to-S (Ps) conversions provide information on the depths to interfaces and the change in seismic properties across the interfaces. To study the amplitude and delay of the Ps phases, recorded three-component teleseismic data are rotated to the theoretical back azimuth to obtain radial and tangential ground motions. The P wave source function is removed by deconvolving the vertical component from the radial and tangential components. Because the seismic signal is teleseismic, there is little energy at frequencies higher than 1 Hz. In accordance, a Gaussian function (e^{-t^2/α^2}, for specified value of α) is convolved with the receiver functions to smooth the high-frequency noise, and the resulting receiver functions are band pass filtered in a frequency band chosen to correspond with the response of the seismometer and the goals of the investigation.

Towards achieving the goals of using receiver functions to resolve interface depths and crustal velocities, two basic problems commonly are encountered. First, the Ps delay time and magnitude depend on combinations of interface depth and the seismic P and S velocities (V_p and V_S, respectively) of the crust above the interface. Specifically, Ps delay time for a ray of near-normal incidence is the product of interface depth and average $V_S^{-1} - V_p^{-1}$ of the overlying crust. Hence absolute depths cannot be estimated without knowledge of crustal P and S wave velocities. The magnitude of the Ps phase does not depend directly on the

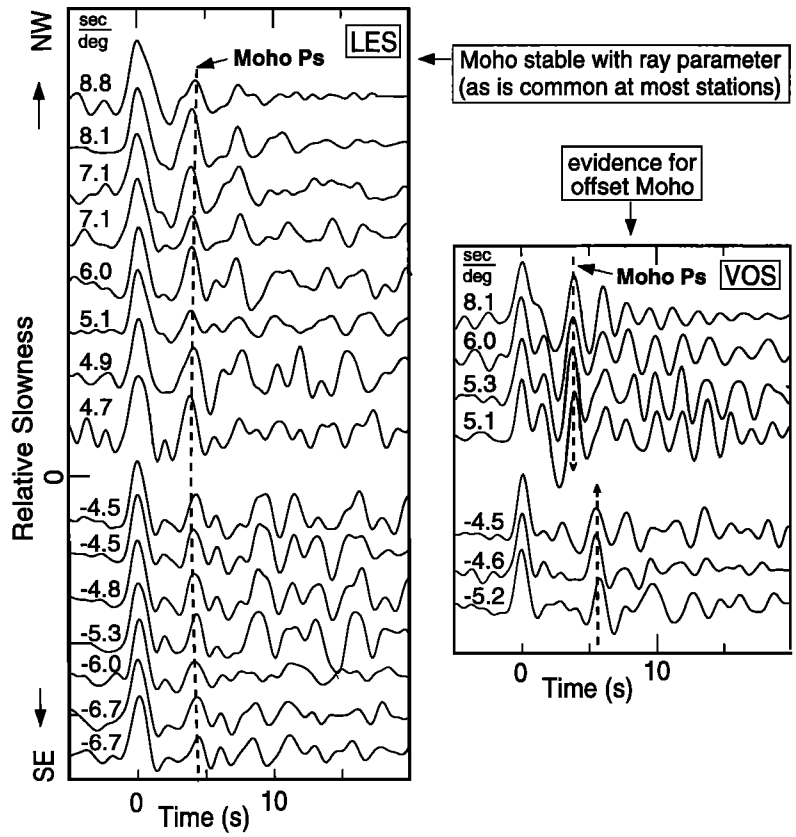

Figure 3. Receiver functions from two stations, for earthquakes of NW and SE back azimuths, ordered by ray parameter. Moho *Ps* phases are indicated with dashed lines (which is slightly curved because a normal moveout correction is included). Station LES is a particularly well-sampled station, and for a wide range in ray geometry, receiver functions are very similar for the duration between the direct *P* arrival (at time equals zero) to the Moho *Ps* arrival, and they show large variations in character after this time. This is typical of most of the stations. In contrast, station VOS is an example that shows an abrupt change in waveform as a function of ray parameter, which is attributed to a large, local change in crustal thickness near this station. Ray parameter, in s/deg, is given for each receiver function. Receiver functions have been band-pass filtered between 0.05 and 1.0 Hz (1-20 s) and convolved with a Gaussian pulse that has a characteristic width of 0.5 s.

absolute value of the velocities above and below the interface, but rather on the seismic impedance across the interface. The main consequence of these limitations is that interface depth is not very well estimated because of the absence of information on absolute crustal velocities. The second basic problem is that reverberatory and direct converted phases may be difficult to distinguish in a receiver function. Reverberations from relatively near surface interfaces (whose fundamental reverberation arrives at times equal to direct *Ps* arrivals from interfaces about 3 times as deep) tend to complicate and mask conversions from the deeper interfaces, and they may be mistaken for direct *Ps* arrivals from deeper interfaces. Hence, without direct information on the near-surface interfaces, ambiguity exists as to which potential interface generated an observed *Ps* arrival.

In spite of these problems with receiver functions, they offer important information that often is difficult to obtain with other techniques. In comparison to the active source experiments, teleseismic *P* wave data have incident angles that are nearly vertical, interact with the deep crustal structure with relatively great energy, and often can be obtained over a great area with relative ease. For these reasons, receiver function deployments provide information that is especially useful in resolving lateral variations in crustal structure and the regional geometry of the Moho. Because the information contained in receiver functions and wide-angle reflection data are rather complimentary, their combined use affords an especially useful means of investigating the crust. Similar advantages can be gained with the combined analysis of receiver functions and surface waves [*Ozalaybey et al.*, 1997].

In our receiver function analysis, we deconvolve by division in the frequency domain and stablize deconvolution by setting the denominator term to a constant absolute value (i.e., "waterlevel" [*Clayton and Wiggins*, 1976]) at any frequency where the spectral amplitude falls below the waterlevel value. A waterlevel usually is chosen to be the maximum spectral amplitude multiplied by 10^{-4}, though in noisy cases the waterlevel is increased to values as great as one tenth of the maximum spectral value. A Gaussian function with $\alpha = 0.5$ s is convolved with the receiver functions, so as to smooth frequencies higher than about 1 Hz (little teleseismic energy occurs at frequencies higher than 1 Hz in the western U.S.). The receiver functions are then band-pass filtered in each of two frequency bands: 0.1-0.4 and 0.05-1 Hz.

The ~350 modelable radial receiver functions are divided into SE, NW, and SW back azimuth groups. Receiver functions to a specific station tend to be very similar in character for events of similar back azimuth, and usually remain similar in character for events of different back azimuths; however receiver functions to a few stations vary considerably as a function of event ray geome-

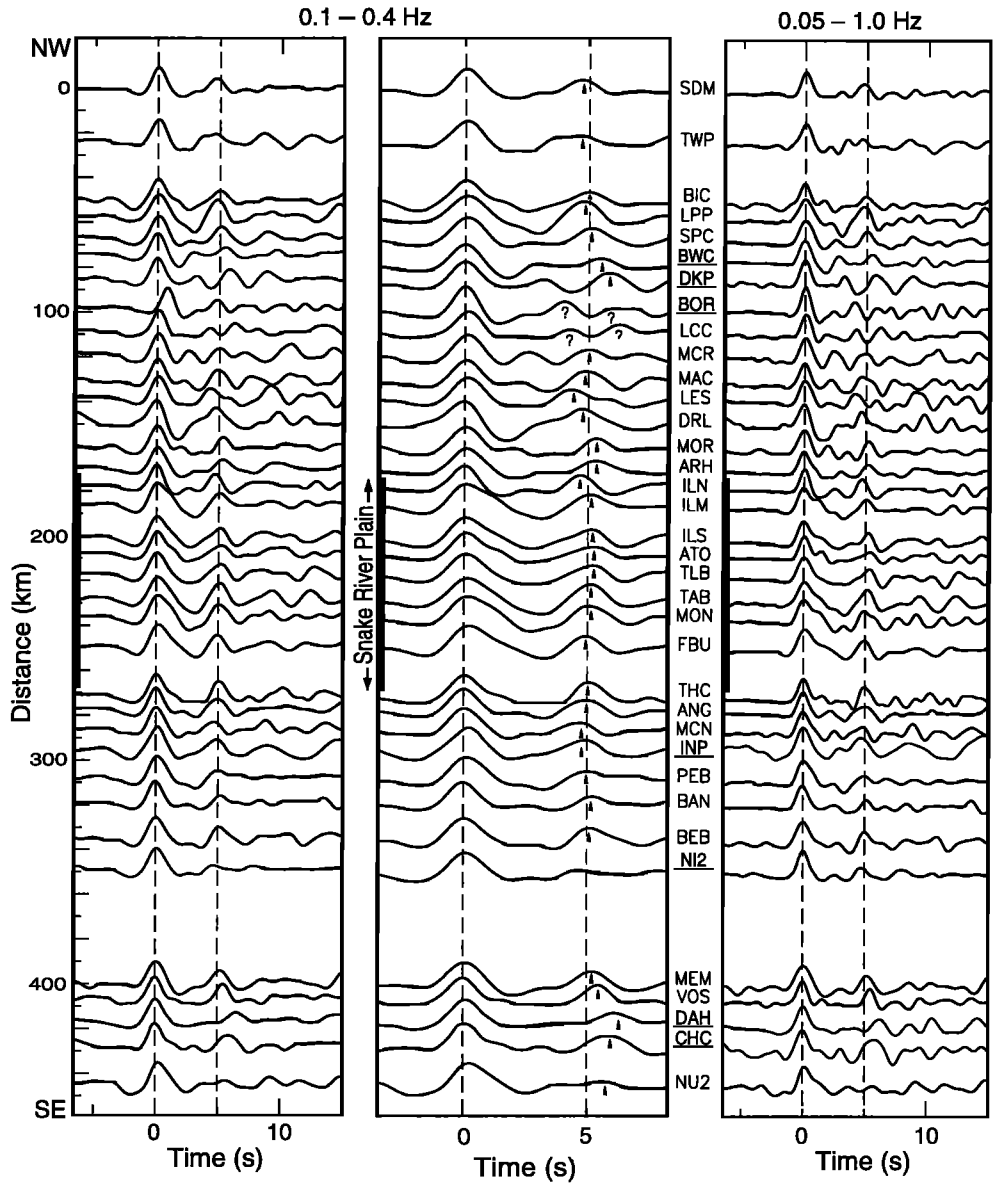

Figure 4. Receiver functions, in two frequency bands. The individual receiver function shown for each station is selected on the basis of its simplicity and representativeness, with preference given to events from SE back azimuths. If no high-quality receiver functions are available from the SE, NW back azimuths are used (and indicated by underlined station names). The origin time is based on the direct *P* wave arrival (i.e., the vertical component of motion). The middle panel shows the Moho *Ps* arrival on a plot with an expanded time scale, and with the Moho *Ps* arrival indicated with arrows. The heavy line indicates the location of the Snake River Plain. Receiver functions have been bandpass filtered as indicated at the top of the figure and convolved with a Gaussian pulse that has a characteristic width of 0.5 s.

try (Figure 3), indicating an abrupt change in crustal structure near such stations. These changes in crustal thickness also can be seen in the record section of receiver functions presented in Figure 4, which shows representative high-quality radial receiver functions from the stations used in this study. Tangential receiver functions are shown and discussed below. The left column of Figure 4 shows the receiver functions bandpass filtered between 0.1-0.4 Hz (2.5-10 s). Prominent arrivals are observed at 4.5-5.8 s across the entire array. These arrivals represent the only major phases in the *P* wave coda in this particular frequency band and are identified as Moho *Ps* conversions. The middle column of Figure 4 shows that the Moho *Ps* phase arrives to the SRP a few tenths of a second later than 5 s, whereas arrivals to either side of the SRP are earlier than 5 s (though arrivals to stations NW of the SRP are not very consistent). On the extreme SE end of our array, in Wyoming, the Moho *Ps* arrivals are very late (~5.8 s).

The right column of Figure 4 shows the same receiver functions bandpass filtered between 0.05-1 Hz (1-20 s). The wider frequency band permits more detailed resolution of the crustal structure. A midcrust *Ps* phase arriving at ~2.5 s, observed in most the off-plain receiver functions (stations SDM-MOR and ANG-NU2), is replaced by a distinctive shoulder at ~1.25 s at most on-plain receiver functions (stations ARH-THC). A consistent (though subtle) *Ps* downswing arrives immediately before a prominent Moho *Ps* for stations on and immediately SE of the SRP. Receiver functions for stations south of NU2 in SE Idaho

(Figure 1) are erratic, and coherent receiver functions could not be derived for these stations. In contrast, receiver functions for stations on the SRP are very stable.

4. Modeling

It is our desire to resolve not only Moho depth beneath our array but also to use our many receiver functions to resolve structure internal to the crust. Several factors work in our favor toward achieving this goal: we have many receiver functions from many closely spaced sites, the receiver functions are usually stable with varying ray geometry and between nearby stations, the on-plain sites are nearly noise free (as seen by the receiver functions in Figure 4 at times prior to the P wave arrival at time = 0), there is good information from the previous wide-angle studies on crustal velocities and interfaces (Figure 2), and the geological history of the region indicates that the crust is a magmatically modified version of the adjacent crust. The fact that receiver functions to on-plain sites have a common character that is distinct from the off-plain sites (Figure 4) suggests that there is a distinctive structure causing this difference, and that this structure is modelable.

We begin modeling by using the crustal velocities and interface geometries resolved previously (Figure 2) [*Sparlin et al.*, 1982; *Chiang and Braile*, 1984] and modifying the interface depths as required to satisfy the receiver functions. The results shown below are the product of an iterative process in which we have made use of forward and inverse modeling.

A stacking of receiver functions recorded at a given site is commonly used to minimize incoherent aspects of the receiver functions. For those stations with many high-quality receiver functions (e.g., Figure 3), we have examined single receiver functions, stacks of receiver functions from similar back azimuths, and the stack of all modelable receiver functions. By stacking receiver functions, we reduce the amount of signal generated by unmodeled sources (such as that created by scattering from irregular topography and sediment-basement interfaces), which can be of large amplitude relative to intercrustal phases. Unfortunately, stacking also degrades the intercrustal phases because, even when these arrivals are seen to be common among several receiver functions, they are not perfectly phase aligned. This is not unexpected since, for the intercrustal phases (which are most clearly observed near frequencies of ~1 Hz), any timing variations of a phase by more than 0.25 s causes stack incoherence. For example, such timing variations will occur for reverberations from a midcrustal layer dipping by as little as ~2°. To contend with this problem, we select receiver functions at each station that are low in pre-arrival noise and display features which are common among receiver functions of similar back azimuth and ray parameter to the same and nearby sites. The chosen receiver functions are those shown in Figure 4. Although we show only these selected receiver functions, all receiver functions to each station have been modeled in order to assess model consistency and stability.

Synthetic receiver functions generated from our initial model (Figure 2) [*Sparlin et al.*, 1982; *Chiang and Braile*, 1984] are similar to the observed receiver functions, leading us to conclude that this is a good choice for the initial structure. During subsequent modeling, velocities and densities are held at the values determined by Sparlin et al. (Figure 2), and layer thicknesses are modified by trial and error until a structure is found that explains the data well while being as close to the initial structure as is possible, and is similar to the structure found at nearby stations. A Thompson-Haskell matrix method [*Haskell*, 1962] is used to calculate the synthetic crustal response functions. Model goodness is evaluated visually by paying attention to those features in the receiver function that are expressed repeatedly for receiver functions of similar ray geometry and location. No attempt is made at modeling the receiver functions after the Moho *Ps* arrival because these phases often vary significantly even among receiver functions of minor variation in back azimuth and ray parameter (Figure 3). We assume a Poisson's ratio of 0.27 [*Christensen*, 1996]. Forward modeling is done initially with the receiver functions filtered in the narrow 0.1-0.4 Hz band, which is especially useful in identifying the Moho arrival. We follow this analysis with modeling of the receiver functions filtered in a broader 0.05-1.0 Hz band in order to address features internal to the crust.

After a crustal structure is estimated by forward modeling, we inverse model the selected receiver functions with an algorithm that seeks the least squares optimal S wave velocity of prescribed layers [*Ammon et al.*, 1990]. V_p is assumed to be $V_S \times \sqrt{3}$ (i.e., Poisson's ratio is 0.25) and density in SI units is calculated using $0.32 \times V_p + 800$ [*Christensen and Mooney*, 1995]. The inversion algorithm iteratively solves for first-order perturbations of V_S about the solution from the previous iteration until suitable convergence is attained in a least squares sense. An initial model needs to be prescribed, and interface depths do not vary.

Inverse modeling often produces layer velocities that are inconsistent with the structure estimated from the forward modeling and the reflection-refraction seismic investigations and that often vary greatly between neighboring stations even when receiver functions are similar. When an initial model is parameterized with many thin layers, modeled velocities tend to produce a sawtooth velocity-depth profile and unreasonably large velocity variations, and receiver functions of similar form can result in very different structures. We stabilize inverse modeling by prescribing thick layers where evidence does not support the existence of thin layers. As an initial structure in inverse modeling, we have used Sparlin et al.'s structure, our forward structure, and other velocity structures. After testing these different initial models, we choose a starting structure based on our forward model. Upper and lower crustal layers are parameterized as thick units, and thin layers are placed near the major crustal boundaries in order to allow the model freedom to change effective layer thickness. Following inversion, we adjust the absolute velocities of the resulting structure to be consistent with the reflection-refraction seismic investigations in such a way as to alter the form of the receiver function as little as possible. This is a straightforward operation since receiver functions are insensitive to absolute velocity.

Figure 5 shows an example in which an inverse model produced midcrustal and lower crustal velocities that are too high (6.8 and 7.2 km/s) compared to the velocities derived from the reflection-refraction studies (Figure 2). We adjust the velocities of the midcrust and lower crust to 6.5 and 6.8 km/s to correspond with those of the refraction experiments while maintaining the large velocity contrast at 10 km that the inverse modeling included to account for observed phases in the receiver functions. The adjusted model accounts for the data equally as well. An example of an inverse-modeled receiver function is shown in Figure 6, compared to the structure determined through forward modeling. The primary difference between forward and inverse models for the on-plain stations is the location of a low-velocity layer, with the inverse modeling locating this layer in the upper crust. The upper crustal low-velocity layer accounts for receiver function phases near the Moho *Ps* arrival with reverberation off the low-velocity layer, whereas during forward modeling we

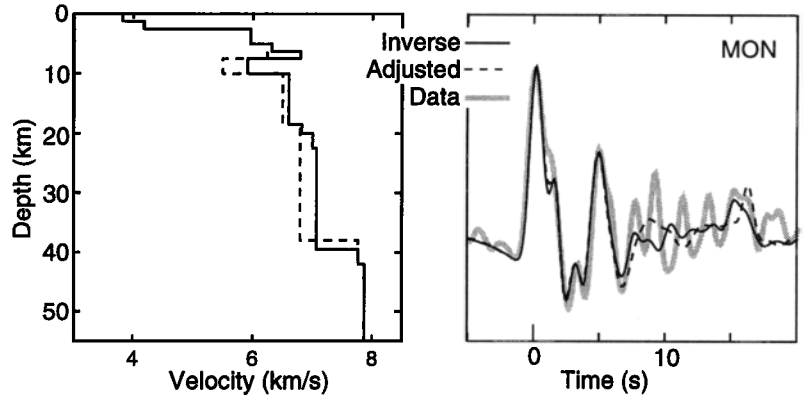

Figure 5. Effects on modeled receiver functions at station MON of manually adjusting the inverse model. The actual receiver function (thick gray line) is compared with the receiver functions generated by the unadjusted inverse model (solid line) and the model adjusted so as to be consistent with the velocities derived from reflection-refraction investigation of the same area [*Sparlin et al.*, 1982] (dashed line). Moho in the adjusted model is pulled up slightly so that the delay of the Moho *Ps* arrival (seen near 5 s) is the same in the inverse and adjusted models. The effects of velocity adjustment on the modeled receiver function is minimal for the Moho *Ps* phase and earlier phases.

model the same waveform character with a direct arrival from a lower crustal low-velocity layer.

Through iterative use of forward and inverse modeling of the selected receiver functions, we derive an estimate of the structure at each site. We then forward model each high-quality receiver function obtained at every site by using the estimated structure as a starting model and varying interface depths as needed to improve the fit between each modeled receiver function and the actual receiver function. Finally, we make minor adjustments to the structure at each station to be as consistent as possible with the set of receiver functions at each station. The variations in modeled structure at each site are used to estimate the uncertainty in the positions of the estimated interfaces. Figure 7 compares the selected receiver functions (shown in Figure 4) with the receiver functions produced by the modeled crust (which are based on the entire set of receiver functions available for each station).

5. Crustal Structure

Figure 8 shows the basic off- and on-plain structure inferred from modeling. The receiver function shown for BAN is typical of off-plain sites. Both forward and inverse modeling produce the off-plain arrival near 5 s with a Moho at depths of ~40 km, and both produce the large ~2.5-s arrival with the combined effects of *Ps* conversion from a midcrustal interface at ~19 km depth and a reverberation from an interface at ~5 km depth. The only required modification to Sparlin et al.'s off-plain structure is a repositioning of the Moho, and the need for such modification is not surprising considering that Sparlin et al. had no seismic information on the off-plain Moho.

We estimate that the Moho lies at ~42 km depth beneath most of the SRP, that the crust thins to less than 40 km beneath the southeastern SRP and adjacent area and thickens to ~47 km where our array crosses into Wyoming. Potential errors in these

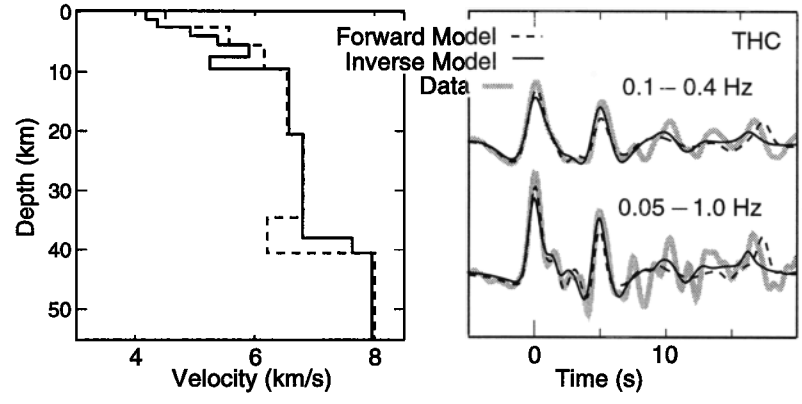

Figure 6. Two crustal structures that satisfy the receiver function for station THC. In forward modeling (dashed line) we include a lower crustal low-velocity layer at this station and most stations in the central portion of the array, whereas inverse modeling (solid line) accounts for the same features in the observed receiver functions (gray line) with reverberations from an upper crustal low-velocity layer. Filter bands as in Figure 4. Although both structures explain the data well, the lower crustal low-velocity layer is more consistent with seismic reflection-refraction results.

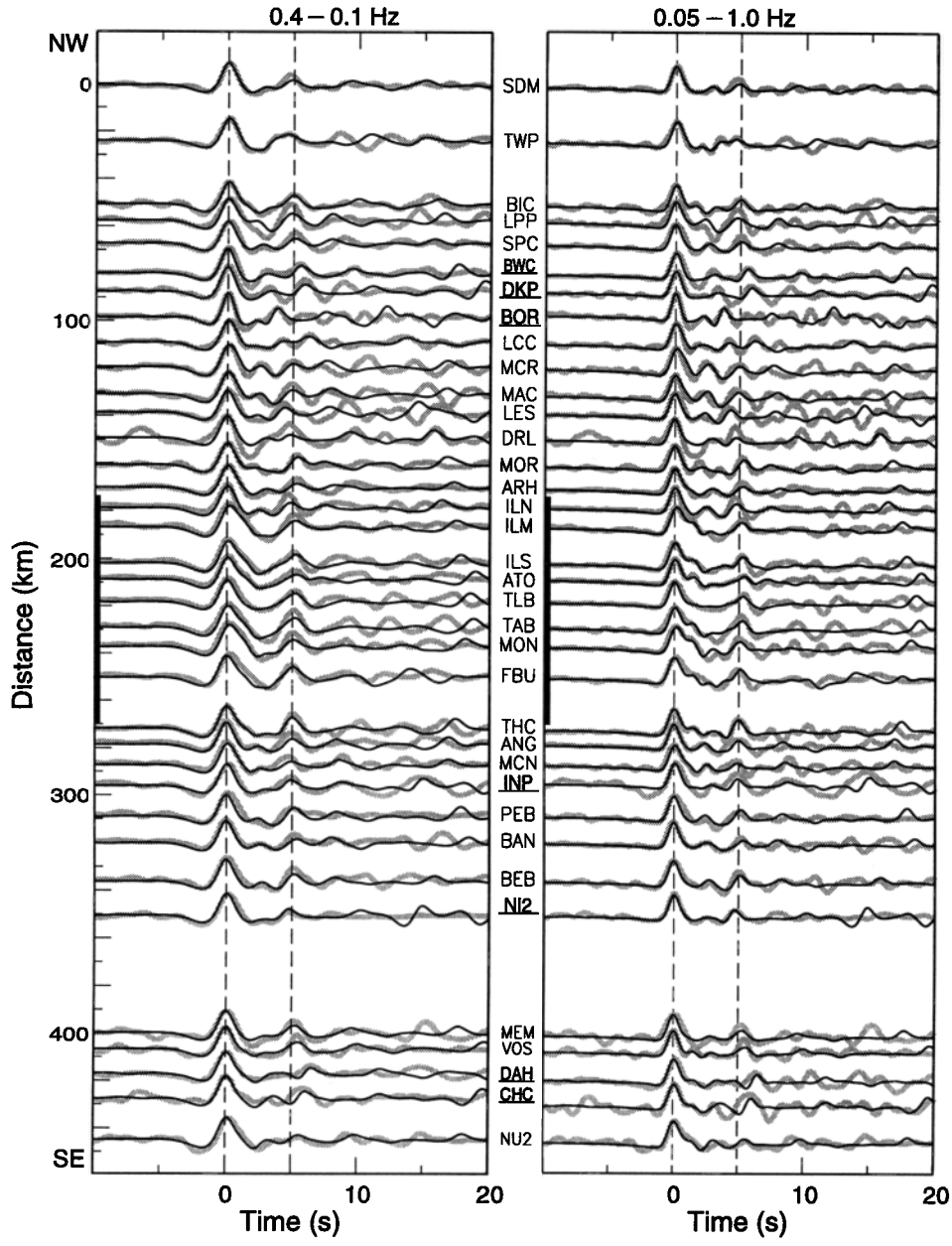

Figure 7. Modeled and observed receiver functions. Conventions as in Figure 4. The receiver functions shown with gray lines are the actual receiver functions shown in Figure 4. Modeled receiver functions (solid lines) result from the crustal structure derived by modeling all the receiver functions to each station, with a starting model from *Sparlin et al.* [1982]. The Moho *Ps* phase arrives near 5 s, and the waveform following the Moho *Ps* arrival is not modeled.

regional estimates of crustal thickness, discussed below, typically are less than ~2 km. Crustal thickening beneath Wyoming results in the large Moho *Ps* delays south of VOS (Figure 4), and the transition in crustal structure near VOS is clear in the back azimuth dependence of receiver functions at VOS (Figure 3). A similar abrupt thickening of the crust to values greater than 40 km was observed in crossing from Utah to Wyoming along a NE oriented refraction line that crosses our array at its southeastern end [*Braile et al.*, 1974].

The station-to-station coherence of receiver functions NW of LES is relatively weak and the crust appears to be complex. Moho depth is most ambiguous in the vicinity of station BOR, where two prominent phases are observed near 5 s (Figure 4). Problems in interpreting these complex receiver functions lead to ambiguity in estimating crustal thickness there. Phases preceding the Moho arrival in this part of the array also are not laterally continuous in any simple way.

The midcrustal phase (seen at 2.5-3.0 s in Figure 4) is common to stations away from the SRP and persists with varying ray parameter, indicating a rather well-developed midcrustal interface near ~19 km depth away from the SRP. Figure 3 illustrates the stability of this phase for an especially well-sampled station (station LES). The prominent midcrustal interface for off-plain sites is consistent with the model shown in Figure 2 [*Sparlin et al.*, 1982].

The on-plain crustal structure of *Sparlin et al.* [1982], as modified by *Chiang and Braile* [1984], is the off-plain crustal structure with two layers added: a thin near-surface low-velocity layer of

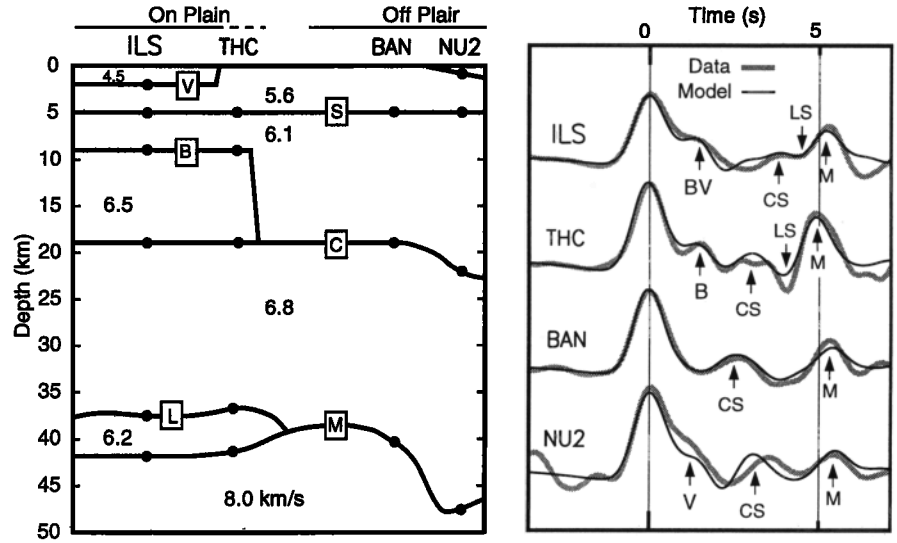

Figure 8. Four receiver functions, showing the general character of receiver functions and the modeled origins of various commonly observed phases. Marked arrivals represent *Ps* arrivals and reverberations from the following interfaces: M, Moho; L, top of low-velocity layer; C, midcrustal interface; B, top of basaltic sill; S, base of Paleozoic sedimentary rocks; and V, base of young volcanic and sedimentary deposits. *P* wave velocities, in km/s, are given in the left panel. In addition to the Moho *Ps* arrival (M at ~5 s) we model the shoulder to the direct *P* arrival (B and BV at ~1.5 s), the positive phase preceding the Moho arrival (CS at 2.5-3.5 s), and the downswing immediately preceding the Moho arrival (LS).

volcanic deposits and a thick midcrustal high-velocity unit interpreted to be a basaltic sill (Figure 2). Although this structure produces receiver functions similar to those observed, our data require several modifications.

5.1. Specific Modifications to Crustal Structure

5.1.1. Basaltic sill. Perhaps the strongest evidence for the sill is found in displacement of the prominent off-plain midcrustal phase found near 2.5 s (arrows in right panel of Figure 9) to about 1.25 s (arrow heads in same figure) for the on-plain data. The top of the basaltic sill generates the ~1.25-s arrival across most the width of the SRP and extending slightly to the south (as indicated by the black bar in Figure 9). The rather constant arrival time of the ~1.25-s phase suggests an approximately flat-topped sill. In Figure 9 our model is seen to produce the shoulder with the combined arrivals of the direct *Ps* conversion from a 10-km-deep interface (the top of the inferred basaltic sill) and the first reverberation of the near-surface layer of volcanic deposits. Either phase alone produces a shoulder with too small an amplitude. Also, removal of the sill results in a large ~2.5 s *Ps* conversion similar to that seen in the off-plain receiver functions and degrades the overall fit prior to ~3 s (Figure 9). Thus receiver function modeling confirms the presence of a high-velocity sill-like structure and its flat top. With respect to the sill, the most important aspect of our modeling is the conclusion that the sill is approximately flat-topped over its entire ~90 km width.

5.1.2. Low-velocity layer. We include a low-velocity layer (LVL) at the base of the crust in our model. This layer is not present in *Sparlin et al.*'s [1982] model but it is present in *Priestley and Orcutt*'s [1982] model of the SRP crust to the NE. Figure 10 shows that for the 11 contiguous stations on or immediately SE of the SRP, inclusion of a LVL at the base of the crust improves the fit of the modeled receiver functions to the actual receiver functions by (1) enlarging the Moho *Ps* phase (by increasing the contrast across the Moho) and (2) generating a downswing immediately prior to the Moho *Ps* arrival (by including an interface with low velocity beneath high velocity immediately above the Moho). The downswing expresses itself either as a distinctive inflection immediately preceding the Moho arrival (e.g., stations ILS-TAB and FBU in Figure 10), or as an unusually large trough (e.g., THC-PEB) when this downswing superimposes with the downswing caused by the reverberation from the base of the Paleozoic sediments. The enlarged Moho phase and precursory arrival are not very profound features, and we take their presence as simply suggestive of a LVL. However, the fit between the observed and modeled receiver functions is improved at all 11 contiguous stations, and it is difficult to reproduce the character of the receiver function at times near 4-5 s without the presence of a LVL.

These receiver functions can be modeled successfully with a LVL either at the base of the crust (as illustrated in Figure 10) or in the upper crust, as is usually created by inverse modeling of these data. Figure 6 shows both options. The lower crustal option is preferred over the ~10-km-deep option because the latter option contradicts the results of *Sparlin et al.* [1982] and *Chiang and Braile* [1984] in an area where their data provide well-resolved images, whereas the lower crust is poorly sampled by their data. Furthermore, refraction data from the Snake River Plain closer to Yellowstone show strong evidence for a low-velocity zone in the lower crust between 20 and 40 km depth, where the low-velocity zone progressively thinning to the SW [*Priestley and Orcutt*, 1982], that is, toward our array.

5.1.3. Nonfault bounded margins of the SRP. Based on modeling of gravity and refraction data, *Sparlin et al.* [1982] infer the presence of a vertical offset fault separating the SRP from the intermontane basins and ranges that trend NW of the SRP. They place this fault between stations ILM and ILS and have it separating a relatively thick ~7 km of sedimentary and volcanic deposits above basement from an accumulation of 2-3 km of deposits to the north (see Figure 2). Our receiver functions fit a model with a uniform 5-km-thick sedimentary layer and overlaying volcanic deposits for all of the stations in this vicinity (results shown with fine arrows in Figure 10), and the fit is degraded considerably

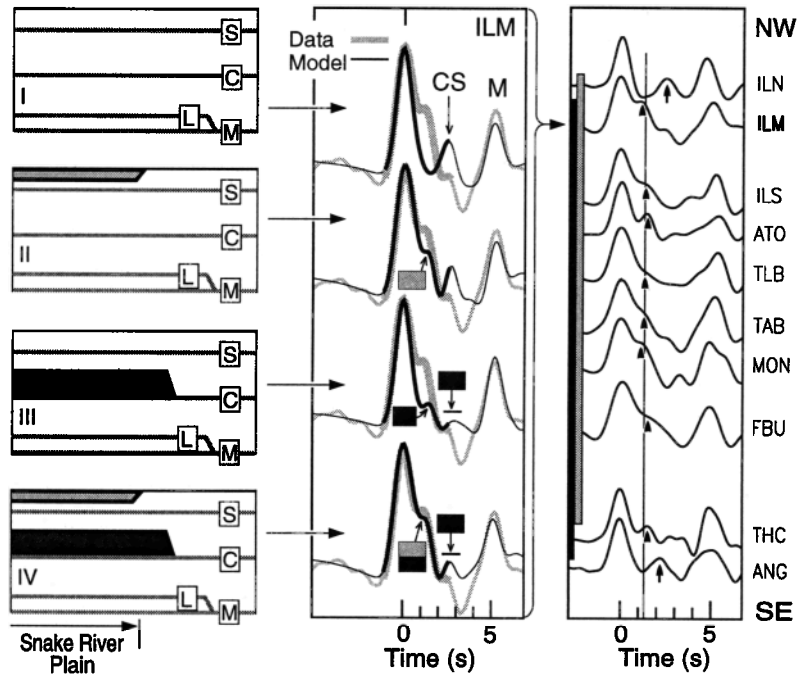

Figure 9. Evidence for a basaltic sill beneath the eastern Snake River Plain. (right) Receiver functions for the stations on or near the Snake River Plain that are well modeled with a basaltic sill, as well as the two adjoining stations (ILN and ANG) that show no evidence for a sill. Arrow heads in this panel indicate the approximately constant arrival time of the *Ps* conversion from the top of the basaltic sill, and complete arrows show the prominent midcrustal arrival that occurs away from the sill. The black bar indicates the range over which the sill conversion is seen, compared to the width of the Snake River Plain, shown with the gray bar. (middle) Actual receiver function for station ILM (gray line) is compared to receiver functions resulting from the various models shown in the left column. (left) Crustal structures include (I) interfaces representing the Moho (M), top of a low-velocity layer (L), a midcrustal boundary (C), and the base of the Paleozoic sediments (S); (II) model I plus a layer of volcanic deposits (gray); (III) model I plus a basaltic sill (black); (IV) model I plus both a layer of volcanic deposits and a basaltic sill. The effect on the receiver functions of each interface is indicated in the middle panel, with bold lines used to emphasize the time duration of interest for the upper crustal phases. The addition of the volcanic layer produces a shoulder at ~1.25 s, as does the inclusion of the basaltic sill. The magnitude of their combined effect depends on the degree to which these phases arrive constructively. The basaltic sill also has the effect of reducing the magnitude of the phase labeled CS, which is prominent whenever the sill is not included, as shown in the middle panel.

when we incorporate thinning of this layer north of the fault. This suggests that a fault of significant offset does not exist in this area. In fact, we find no evidence in our data that our array crosses a fault anywhere near the Snake River Plain. Since our array extended NW of the SRP within an intermontane basin, we suggest that the upper crust continues horizontally from the SRP into the basins, and that the basin-bounding mountain ranges are upwarped above the SRP. This is consistent with *Anders and Schlische* [1994] and N. McQuarrie and D. Rodgers [Subsidence of a volcanic basin by flexure and lower crustal flow – the eastern Snake River Plain, Idaho, submitted to Tectonics, June, 1997], who report that near the SRP a strong downwarping of the mountain ranges toward the SRP occurs.

5.2. Uncertainties

Figure 11a shows our modeled crustal structure along the length of the seismic array. Our modeled crustal structure and analysis of uncertainties along the length of the seismic array are presented in Figure 11a. Absolute and relative uncertainties exist in this estimated structure owing to three classes of potential error: (1) a misprescription of seismic parameters (V_p and Poisson's ratio), (2) data noise and small-scale structure, and (3) difficulty in interpreting complex receiver functions. The availability of preexisting P wave velocity structure [*Sparlin et al.*, 1982; *Chiang and Braile*, 1984] (Figure 2) not only provide the information needed to constrain the depth-velocity trade-off but supply the specific knowledge on interfaces that allows us to distinguish direct *Ps* conversions from reverberations.

With knowledge on absolute crustal velocities, interface depths are estimated well. For instance, if the 20-km-thick lower crust were of velocity 6.6 km/s (instead of 6.8 km/s), Moho depth would be mislocated by 0.6 km. An erroneous choice of Poisson's ratio could have a somewhat larger effect; if a Poisson's ratio of 0.25 were correct for the lower half of the crust, and a value of 0.27 were chosen, Moho depth would be mislocated by 1.2 km. Thus reasonable variations in seismic parameters may cause up to about 2 km of error in Moho depth estimate (and less effect on shallower interfaces). This class of uncertainty (i.e., those resulting from imperfect knowledge of seismic parameters), by affecting nearby stations similarly, would tend to have more effect on the depth to interfaces than it would on local variation in interface geometry.

A more serious problem is model inconsistency owing to data noise and small-scale crustal heterogeneity. This source of uncertainty is assessed by modeling receiver functions for all available events at each station and examining the range in modeled inter-

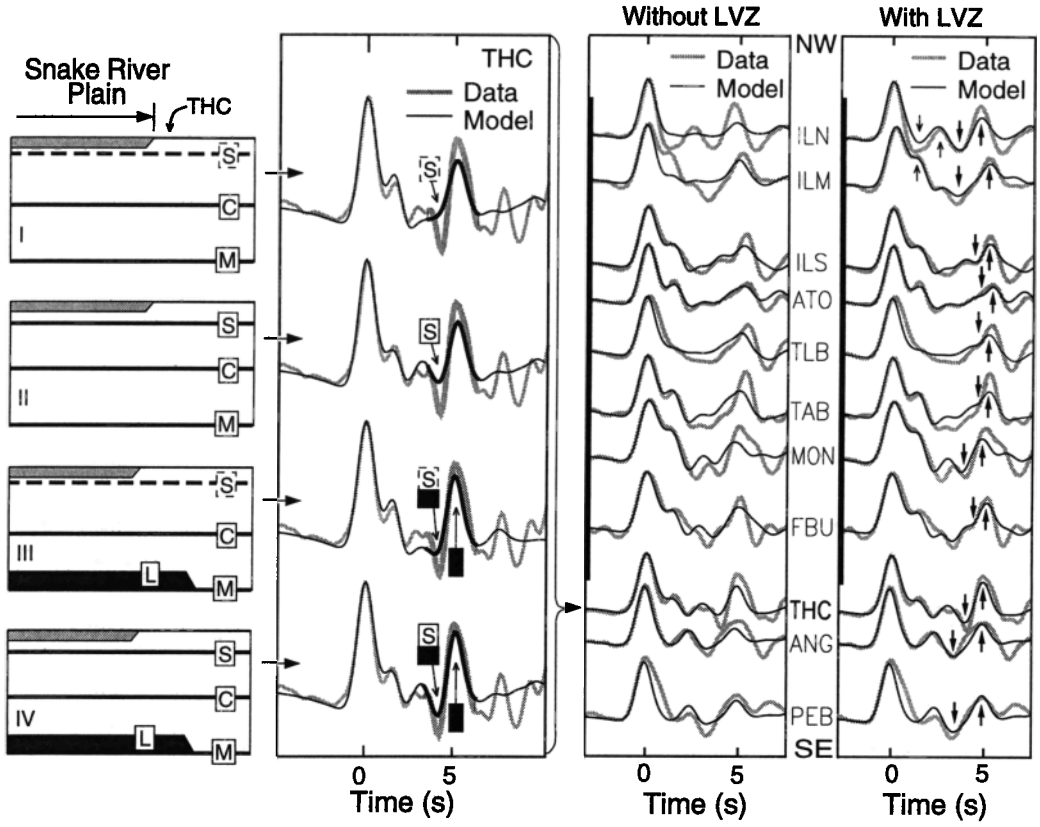

Figure 10. Evidence for a low-velocity layer at base of crust beneath the eastern Snake River Plain. The right panel shows the effect of including the low-velocity layer (triangle-head arrows) for those stations that show evidence for this layer. The panel second from left shows the effects on the receiver function (at station THC) of including the structures shown in the left panel: (I) The receiver function calculated by the model with improperly located S interface and without a low-velocity layer (LVL). (II) The receiver function calculated by the model with properly located S interface and without LVL. This produces a well-timed downswing that proceeds the Moho *Ps* arrival. (III) The receiver function calculated by the model with improperly located S interface and LVL. (IV) The receiver function calculated by the model with properly located S interface and LVL. This produces both a downswing that proceeds the Moho *Ps* arrival and an upswing that increases the amplitude of the Moho arrival. As shown in the right panel, the LVL improves the fit to the receiver functions for all stations shown in this figure by enlarging the Moho arrival and producing a downswing or inflection ~1 s prior to the Moho arrival. Also shown (with open-head arrows on stations ILN and ILM) is the effect of omitting (right panel) and including (panel second from right) a fault near the northern side of the Snake River Plain suggested by *Sparlin et al.* [1982].

face depth. More specifically, our estimate of uncertainty for a particular interface beneath a particular station is the standard error in the modeled interface depth at this station and the two neighboring stations (excepting cases where where stations are separated by more than 15 km). This involves anywhere from 2 to 35 receiver functions. These uncertainty estimates are shown in Figure 11b, plotted at 2 standard errors. Uncertainty in the location of the top of the LVL is shown relative to the Moho, whereas errors in the depths of other interfaces are shown relative to the Earth's surface.

Because most of our events are of SE back azimuth, we have chosen to emphasize these examples in the figures shown in this paper. Near station BOR (Figures 1 and 4) the receiver functions are of relatively poor quality. For this area, receiver functions for events of NW back azimuth are of higher quality, and we show these in Figures 4 and 7. The resulting structure for this area is complex, and where ambiguity in Moho depth occurs we show both possibilities and assign large uncertainties (Figure 11b).

5.3. Tangential Energy

Tangential waveforms often contain significant energy, suggesting anisotropy in the crust, dipping interfaces, or scattering from surface or near-surface structure. Figure 12 shows representative tangential receiver functions for events of SE back azimuth. Tangential receiver functions for the off-plain stations tend to be much more energetic than are those for on-plain stations. The extremely low amplitudes of tangential receiver functions observed on the SRP stations indicates that SRP crustal interfaces do not dip strongly and that this crust is not strongly anisotropic.

The greatest tangential amplitudes occur near the NW end of the array, in the same general region where the radial receiver functions are least coherent (Figure 4) and crustal structure most poorly resolved (Figure 11). Because tangential energy is most prevalent at sites on deep sedimentary basins and near rugged topography, wave field refraction and scattering from basin structure [*Owens and Crossen*, 1988] and topography is considered a

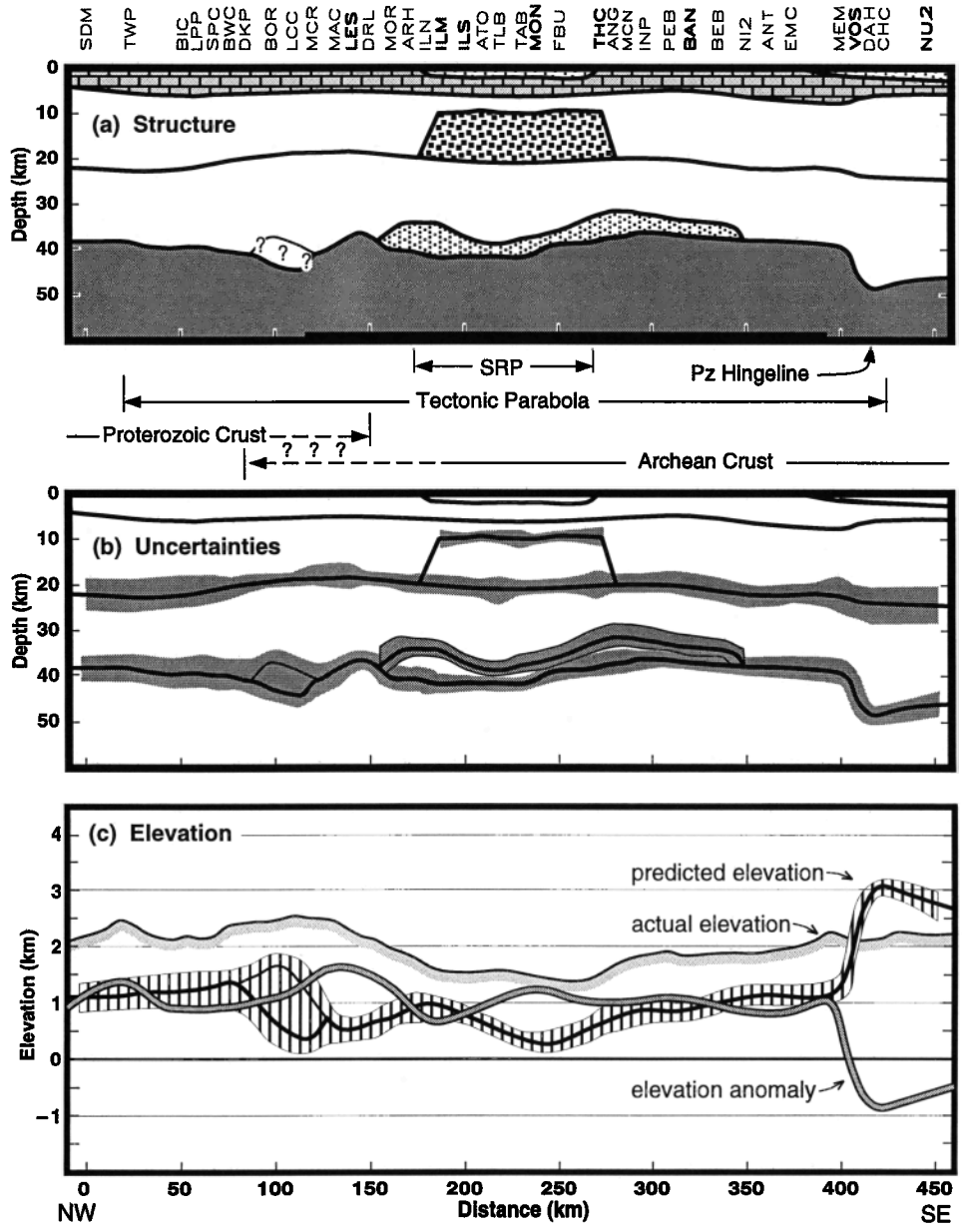

Figure 11. (a) Crustal structure. The structure shown is modified from an initial model presented by *Sparlin et al.* [1982] as required to account for our receiver functions. Young near-surface volcanic and sedimentary deposits (light stippled pattern) are underlain by Paleozoic sediments (brick pattern) and a granitic upper crust. A sill-like body (heavy stipple pattern) occupies the lower portion of the upper crust beneath the Snake River Plain. The lower crust is shown with a low-velocity layer of presumed partial melt (dot pattern) distributed over a portion of its base. Crustal thickness increases SE of a boundary defined by two nearly coincident trends: the Paleozoic hingeline ("Pz Hingeline" in figure) and the SE margin of the tectonic parabola. The Moho is difficult to identify at places NW of the Snake River Plain and is especially ambiguous in the Borah Peak area (near station BOR). In this figure we choose to emphasize the deeper of two possible Moho locations because this choice is more consistent with the topography and the probable occurrence of a crustal suture in this region [*Erslev and Sutter*, 1990; *Houston et al.*, 1993]. Station locations shown with bold letters indicate stations illustrated in previous figures. The range of structure shown by *Sparlin et al.* [1982] (Figure 2) is indicated with heavy bar at bottom. (b) Uncertainties in crustal structure. Uncertainties of important interfaces, shown at 2 standard errors, are indicated with the gray pattern. The uncertainties are relative to the Moho for the top of the low-velocity layer and relative to the Earth's surface for the other interfaces. (c) Elevations. We use a density structure modified from *Sparlin et al.* [1982] to predict the elevation (solid line overlaying a ruled pattern representing the uncertainties), assuming this crust lies on an "average" upper mantle (discussed in text). The difference between the actual elevation and the predicted elevation yields an elevation anomaly. Over the width of the tectonic parabola the elevation is ~1 km too high, whereas to the SE of the tectonic parabola (and Paleozoic hingeline) the elevation is ~0.5 km too low. These elevation anomalies are attributed to lateral variations in mantle density.

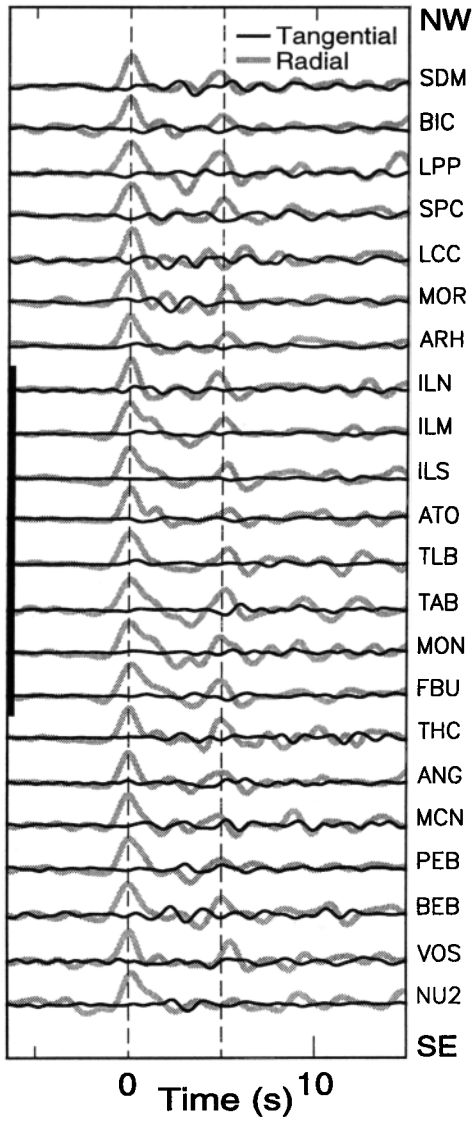

Figure 12. Tangential and radial receiver functions for SE arrivals. The amplitudes of the tangential receiver functions, which should be zero for isotropic, flat-lying, planar layers, are seen to vary from small values for sites on the Snake River Plain to moderate and large values for sites off of the Snake River Plain.

probable origin. The absence of a clear time separation between radial and tangential phases suggests that crustal anisotropy is not a likely origin of tangential energy beneath our array (in contrast to results elsewhere in the Basin and Range [*McNamara and Owens*, 1993; *Peng and Humphreys*, 1997]). At several of the off-plain stations, tangential phases for arrivals of opposing back azimuth are observed to change sign. This suggests that the causative interface dips with a component of dip out of the plane of the incident rays [*Langston*, 1977; *Baker et al.*, 1997; *Peng and Humphreys*, 1997]. If this is so, then some of the *P* wave energy will be projected onto the horizontal components and may be misinterpreted. Because of likely problems with dipping structure and scattered arrivals at many of the off-plain stations, only the main features of the receiver functions (i.e., the Moho and midcrustal arrivals) are considered well constrained there. This is consistent with our modeling.

6. Discussion

6.1. Seismic Structure

Perhaps the most significant aspect of our work is resolution of Moho depth and depth variations across the Yellowstone swell (including the SRP) and, to the SE, slightly beyond. At ~40 km, crustal thickness beneath the swell is near global average [*Christensen and Mooney*, 1995], although its thickness is 5 or more kilometers greater than the crust in the rest of the Basin and Range [*Braile et al.*, 1989; *Pakiser*, 1989]. Where our array leaves the Basin and Range and crosses into Wyoming, a thickening of the crust to ~47 km marks a transition to the rather great thicknesses typical of the Rocky Mountains [*Braile et al.*, 1989; *Sheehan et al.*, 1995].

North of the SRP, apparent crustal complexity creates receiver functions that are difficult to model (Figure 7), and the crust may be considerably more heterogeneous than represented in Figure 11a. Our problems with modeling this region are compounded by the fact that little previous seismic work has been done in this region. *Sparlin et al.* [1982] have essentially no seismic data for the area north of the SRP. *Sheriff and Stickney* [1984] model local blast data along a line trending NE from station BIC into Montana. They model these data with a crust about 33 km thick and with velocities in the lower crust of about 5.9 km/s. This structure is inconsistent with our results at BIC (which has a well-formed Moho *Ps* arrival at 5 s) and most nearby stations. Receiver function phases that arrive at times representative of the midcrust are not simple, and in the region between stations MOR and BIC there are hints of dipping crustal features. The crust beneath the NW part of our study contains a transition between Archean and Proterozoic basement rock (suture or major change in metamorphic grade [*Houston et al.*, 1993]). It also crosses the SW extrapolation of the Madison Mylonite Zone, a major Proterozoic shear zone exposed north and west of Yellowstone that trends parallel to the SRP [*Erslev and Sutter*, 1990; *Houston et al.*, 1993]. Hence the complexity in receiver functions from this area may well reflect the complex Precambrian structure of the crust. However, in the absence of additional seismic information on the structure internal to the crust beneath this part of our array, we simply assume a two-layer crust and direct our effort at resolving Moho depth.

The crust SE of the SRP thins to ~37 km and thickens considerably near where our array crosses the Wyoming border. This crustal thickness in SW Wyoming is similar to that of *Braile et al.* [1974], and the trend toward thickening to the east was found in *Willden*'s [1965] early refraction study (seismic line shown in Figure 1). However, at 31 km beneath the SRP and 37 km beneath Flaming Gorge, Utah, Willden's low estimate of crustal thickness is inconsistent with both *Braile et al.*'s [1974] and our own study.

6.2. Isostasy

By assigning densities to the crustal layers, and assuming local isostasy, we estimate an elevation anomaly with respect to a reference continental mantle lithosphere. Our reference lithosphere is an average of the near sea level margin of the United States along the Atlantic and Gulf of Mexico, for which *Braile et al.* [1989] give an average crustal thickness of 30 km (i.e., the crustal load holds the top of the mantle at a depth of 30 km) and an average crustal *P* wave velocity of 6.4 km/s (from which we infer an average crustal density of 2840 kg/m^3, using the work by *Christensen*

and Mooney [1995]). Figuratively speaking, we place the crust from our field area on this reference mantle and use isostasy to calculate an elevation anomaly. This represents the lateral buoyancy structure of the mantle in our area compared to the reference mantle.

To estimate the crustal load in our field area, we start with the densities given by *Sparlin et al.* [1982] and our crustal structure, modify the density of the midcrustal sill-shaped body, assign a density to the low-velocity lower crust, and then estimate an amount of density reduction arising from the elevated crustal temperatures in the area of elevated heat flow. Emplacement of the midcrustal body probably occurred beneath a Yellowstone-like magmatic system, where hot conditions would cause a slow cooling and crystalization of basaltic magmas to gabbros. If so, and if the actual velocity of this body is near 6.5 km/s (as estimated by *Sparlin et al.* [1982] and *Chiang and Braile* [1984]), then gabbroic intrusions ($V_p \approx 7.1$ km/s [*Christensen and Mooney*, 1995]) and the granite-granodiorite country rock (of velocity measured at $V_p = 6.1$ km/s adjacent to the SRP [*Sparlin et al.*, 1982]) would need to be proportioned approximately equally. Such a gabbro-granodiorite composite would have an average density of about 2830 kg/m^3 [*Christensen and Mooney*, 1995], which is 50 kg/m^3 less dense than the value assumed by *Sparlin et al.* [1982]. The isostatic effect of modifying the sill density is to increase the predicted SRP elevation by about 0.17 km. We assign a density to the volume of presumed partial melt in the lowermost crust that is 50 kg/m^2 less dense that the unmolten lowermost crust, which is equivalent to this rock being 10-15% partially molten. This contributes an additional 0.05-0.10 km of uplift.

The final density adjustment is made to account for thermal expansion of the heated crust (compared to more typical continental crust, upon which standard density-velocity relations are based [e.g., *Christensen and Mooney*, 1995]). We assume that the SRP and the region extending ~70 km SE along our array has unusually hot crust. This is based on the mutually consistent distributions of young magmatism, high heat flow and geothermal activity [*Blackwell and Steele*, 1992], and the inferred distribution of lower crustal partial melt (Figure 10). To calculate the effect of local heating, we assume that the Moho temperature beneath this region is 250°C hotter than elsewhere and that this temperature difference diminishes linearly to zero at the Earth's surface. The value of 250° is chosen to be consistent with the heat flow in the region SE of the SRP, which is ~20 mW/m^2 greater than that found away from these regions (i.e., in SW Wyoming and central Idaho) [*Blackwell and Steele*, 1992]. Heat flow through the SRP is greater by an additional ~20 mW/m^2. We do not include additional thermal density reduction of the SRP crust because we have little sense of the crustal thermal structure there; simple extrapolation of this gradient leads to unreasonably large Moho temperatures, and large-scale groundwater flow influences the near-surface temperature field [*Blackwell and Steele*, 1992]. With any reasonable choice of crustal rock type [*Christensen and Mooney*, 1995], thermal expansion results in surface uplift of ~0.35 km. A lesser or greater temperature difference would have a corresponding effect on crustal density and uplift.

Figure 11c shows the predicted elevations compared to the actual elevation (averaged over a 70-km-wide swath centered on our array, so as to average over the 35-km wavelength of the basins and ranges in this area). The elevation NW of the Paleozoic hingeline (i.e., over the width of the tectonic parabola) stands about 1 km higher than our reference lithosphere, whereas the elevation south of the hingeline is 0.5 km lower than this reference. Using a standard oceanic crustal structure (water over basalt of density 3000 kg/m^3) and age-subsidence relation (depth $= 2.5 + 0.38\sqrt{t}$ for age in million years and depth in kilometers), an excess elevation of 1 km would be supported by an oceanic mantle that is about 12 m.y. old. This suggests that there is little mantle lithosphere remaining beneath the area of the Yellowstone swell. The uncertainties in calculated elevation resulting from uncertainties in crustal thickness are roughly ±200 m, as shown in Figure 11c.

6.3. Speculations

The SRP crust does not appear to be greatly thickened compared to the crust adjacent to the SRP, in spite of the great volumes of magma added to the crust in the form of the midcrustal "basaltic sill" and any lower crustal addition or underplate. However, the crust in this part of the Basin and Range is 5-10 km thicker than Basin and Range crust elsewhere. This combination of observations leads us to suggest that the lower crust beneath the SRP flowed laterally away from the SRP (as considered by *Anders and Sleep* [1992]). Any such flow would contribute to the temporal subsidence of the SRP (which has been attributed to cooling [*Brott et al.*, 1981]).

The Paleozoic hingeline (Figure 1) has been the boundary of tectonic and igneous events repeatedly during the Phanerozoic. It originated during marginal downwarp of the continent following continental rifting near the end of the Precambrian, and marginal subsidence reflects lithospheric cooling and thickening [*Sleep*, 1971; *Karner and Watts*, 1982]. Hence this lithosphere (whatever is left of it) probably is compositionally distinct from the older lithosphere east of the hingeline that presumably is more typical of older cratonic mantle [*Jordan*, 1981], that is, depleted of basaltic component. It is in heading east across the Paleozoic hingeline that the currently observed abrupt thickening of the crust, strengthing of the lithosphere [*Lowry and Smith*, 1994], and increase in mantle density occurs. The hingeline currently separates the Basin and Range from the Rocky Mountains near the southeast end of our array. It also is close to the current eastern margin of the Yellowstone swell and the tectonic parabola (Figure 1). This is interesting because the margin of the Yellowstone swell and the tectonic parabola are features generally attributed to ongoing sublithospheric activity [e.g., *Anders and Sleep*, 1992; *Pierce and Morgan*, 1990] and not to older, inherited structure.

7. Conclusion

Building on previous studies (especially *Sparlin et al.* [1982]), receiver function analysis has yielded the crustal structure shown in Figure 11a for the eastern SRP and nearby regions. Combined use of wide-angle and receiver function techniques, by complimenting one another, provide an especially powerful tool for the investigation of this crust. When we combine our results with studies along the axis of the Snake River Plain and Yellowstone, a general view emerges, which is illustrated in Figure 13. Magmatic activity propagating with the Yellowstone hotspot has injected basaltic melt into the crust to depths as shallow as ~10 km, thereby creating the midcrustal "basaltic sill." With time, the top of the partial melt zone descends to greater depth (resulting from cooling and lower crustal flow), so that ~70 km SW of Yellowstone it lies at a depth of ~20 km [*Priestley and Orcutt*, 1982] and at the location of our array it lies at a depth of ~35 km. The load of the upper crustal basaltic intrusion depresses the crust by an amount sufficient to account for the physiographic SRP downwarp, which we suggest was accommodated by lower crustal

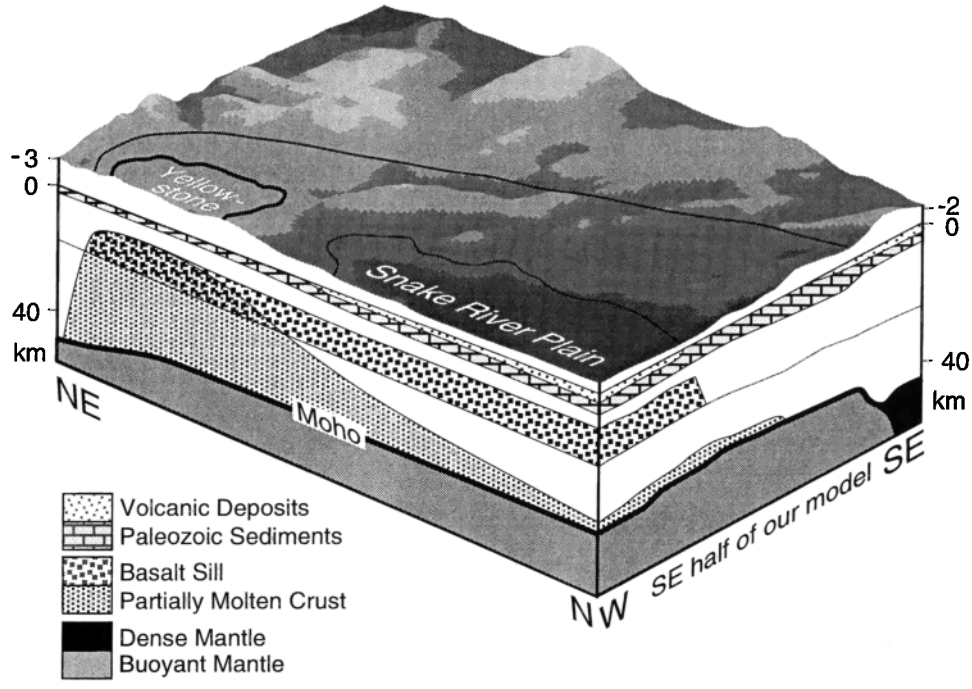

Figure 13. Representation of inferred crustal structure in the vicinity of Yellowstone and the eastern Snake River Plain. View is to the SE. Shading indicates relief. The outermost line is the outer limit of the tectonic parabola (and, for the region shown, the approximate location of the Paleozoic hingeline); the inner lines represent the Snake River Plain (finer line) and the Yellowstone Caldera (heavy line). The left exposed face trends near the axis of the Snake River Plain, and the right exposed face trends beneath the SE portion of our experiment. The zone of lower crustal partial melt is shown increasing in thickness towards Yellowstone, where it is involved in the construction of the presumed basaltic sill (consistent with our results and the findings of *Priestley and Orcutt* [1982] for the area near the NE termination of the Snake River Plain). The crust NE of Yellowstone is inferred to thicken to values more typical of Wyoming; thinning to the SW is a result of prior extension west of the Paleozoic hingeline. A major increase in mantle density to the SE is indicated by dark gray.

flow. We find no evidence that SRP subsidence is associated with major faults bounding the margin of the SRP.

While the general physiography across the width of the Yellowstone swell is well explained by variations in crustal structure, the crust across the width of the Yellowstone swell is maintained at anomalously high elevation by a mantle that is approximately uniformly buoyant and positively buoyant compared to the mantle beneath Wyoming (Figure 13). The relatively great net buoyancy of the mantle beneath the Yellowstone swell precludes a significant thickness of mantle lithosphere there. The transition from this buoyant upper mantle to a mantle buoyancy more typical of old lithosphere occurs at a location defined by both (1) the SE margin of the tectonic parabola (i.e., the inferred margin of the Yellowstone swell) and (2) a Paleozoic-age hingeline associated with old continental rifting. It is difficult to know which of these features is more fundamental to the origin of the mantle contrast.

Acknowledgments. We thank Ken Dueker for many discussions on the topics discussed in this paper, and for operating the PASSCAL array that obtained the data that we used. Chuck Ammon kindly provided us his inversion code. We appreciate helpful reviews from Randy Keller, Larry Braile and an anonymous reviewer, which improved this manuscript. This research was funded under NSF grants EAR-9206565 and EAR-9405547 and made possible by the availability of seismic instrumentation supplied by the PASSCAL component of the IRIS consortium.

References

Ammon, C. J., The isolation of receiver effects from teleseismic *P* waveforms, *Bull. Seismol. Soc. Am., 81*, 2504-2510, 1991.

Ammon, C. J., G. E. Randall, and G. Zandt, On the nonuniqueness of receiver function inversions, *J. Geophys. Res., 95*, 15,303-15,318, 1990.

Anders, M. H., and R. W. Schlische, Overlapping faults, intrabasin highs, and the growth of normal faults, *J. Geol., 102*, 165-180, 1994.

Anders, M. H., and N. H. Sleep, Magmatism and extension: The thermal and mechanical effects of the Yellowstone hotspot, *J. Geophys. Res., 97*, 15,379-15,393, 1992.

Anders, M. H., J. W. Geissman, L. A. Piety, and J. T. Sullivan, Parabolic distribution of circumeastern Snake River Plain seismicity and latest Quaternary faulting, migratory pattern and association with the Yellowstone hotspot, *J. Geophys. Res., 94*, 1589-1612, 1989.

Baker, G. E., J. B. Minster, G. Zandt, and H. Gurrola, Constraints on crustal structure and complex Moho topography beneath Pinion Flat, California, from teleseismic receiver functions, *Bull. Seismol. Soc. Am., 86*, 1830-1844, 1997.

Blackwell, D. D., and J. L. Steele, Geothermal map of North America, in *The Decade of North American Geology, Map-006*, Geol. Soc. of Am., Boulder, Colo., 1992.

Braile, L. W., R. B. Smith, G. R. Keller, R. M. Welch, and R. P. Meyer, Crustal structure across the Wasatch Front system from detailed seismic refraction studies, *J. Geophys. Res., 79*, 2669-2677, 1974.

Braile, L. W., R. B. Smith, J. Ansorge, M. R. Baker, M. A. Sparlin, C. Prodehl, M. M. Schilly, J. H. Healy, St. Mueller, and K. H. Olsen, The Yellowstone-Snake River Plain seismic profiling experiment: Crustal structure of the eastern Snake River Plain, *J. Geophys. Res., 87*, 2597-2609, 1982.

Braile, L. W., W. J. Hinze, R. R. B. von Freese, and G. R. Keller, Seismic properties of the crust and uppermost mantle of the conterminous United States and adjacent Canada, in *Geophysical Framework of the Continental United States*, edited by L. C. Pakiser, and W. D. Mooney, *Mem. Geol. Soc. Am., 172*, 655-680, 1989.

Brott, C. A., D. D. Blackwell, and J. P. Ziagos, Thermal and tectonic implications of heat flow in the eastern Snake River Plain, Idaho, *J. Geophys. Res., 86*, 11,709-11,734, 1981.

Burdick, L. J., and C. A. Langston, Modeling crustal-structure through the use of converted phases in teleseismic body-waveforms, *Bull. Seismol. Soc. Am., 67,* 677-691, 1977.

Chiang, C. S., and L. W. Braile, An example of two-dimensional synthetic seismogram modeling, *Bull. Seismol. Soc. Am., 74,* 509-519, 1984.

Christensen, N. I., Poisson's ratio and crustal seismology, *J. Geophys. Res., 101,* 3139-3159, 1996.

Christensen, N. I., and W. D. Mooney, Seismic velocity structure and composition of the continental crust: A global view, *J. Geophys. Res., 100,* 9761-9788, 1995.

Clayton, R. W., and R. A. Wiggins, Source shape estimation and deconvolution of teleseismic bodywaves, *Geophys. J. R. Astron. Soc., 47,* 151-177, 1976.

Erslev, E. A., and J. F. Sutter, Evidence of Proterozoic mylonitization in the northwestern Wyoming province, *Geol. Soc. Am. Bull., 102,* 1681-1694, 1990.

Haskell, N. A., Crustal reflection of plane *P* and *SV* waves, *J. Geophys. Res., 67,* 4751-4767, 1962.

Houston, R. S., et al., The Wyoming Province, in *The Geology of North America*, vol. C2, *Precambrian: Conterminous U.S.*, edited by J. C. Reed et al., pp. 121-170, Geol. Soc. of Am., Colo., 1993.

Jordan, T. J., Continents as a chemical boundary layer, *Philos. Trans. R. Soc. London, Ser. A, 301,* 359-373, 1981.

Karner, G. D., and A. B. Watts, On isostasy at Atlantic type margins, *J. Geophys. Res., 87,* 2923-2948, 1982.

Langston, C. A., The effect of planar dipping structure on source and receiver responses for constant ray parameter, *Bull. Seismol. Soc. Am., 67,* 1029-1050, 1977.

Langston, C. A., Structure under Mount Rainier, Washington, inferred from teleseismic body waves, *J. Geophys. Res., 84,* 4749-4762, 1979.

Lowry, A. R., and R. B. Smith, Flexural rigidity of the Basin and Range-Colorado Plateau-Rocky Mountain transition from coherence analysis of gravity and topography, *J. Geophys. Res., 99,* 20,123-20,140, 1994.

McNamara, D. E., and T. J. Owens, Azimuthal shear wave velocity anisotropy in the Basin and Range Province using Moho *Ps* converted phases, *J. Geophys. Res., 98,* 12,003-12.017, 1993.

Morgan, W. J., Deep mantle convection plume and plate motions, *Am. Assoc. Pet. Geol. Bull., 56,* 203-213, 1972.

Owens, T. J., and R. S. Crossen, Shallow structure effects on broadband teleseismic *P* waveforms, *Bull. Seismol. Soc. Am., 78,* 96-108, 1988.

Ozalaybey, S., M. K. Savage, A. F. Sheehan, J. N. Louie, and J. N. Brune, Shear-wave velocity structure in the northern Basin and Range Province from the combined analysis of receiver functions and surface waves, *Bull. Seis.. Soc. Am., 87,* 183-199, 1997.

Pakiser, L. C., Geophysics of the Intermontane system, in *Geophysical Framework of the Continental United States*, edited by L. C. Pakiser, and W. D. Mooney, *Mem. Geol. Soc. Am.*, 172, 235-247, 1989.

Peng, X., and E. D. Humphreys, Moho dip and crustal anisotropy in northwestern Nevada from teleseismic receiver functions, *Bull. Seismol. Soc. Am., 87,* 745-754, 1997.

Pierce, K. L., and L. A. Morgan, The track of the Yellowstone hotspot: Volcanism, faulting, and uplift, *U.S. Geol. Surv. Open File Rep., 90-415,* 1-48, 1990.

Poole, F. G., et al., Latest Precambrian to latest Devonian time; Development of a continental margin, in *The Geology of North America*, vol. G3, *The Cordilleran Orogen: Conterminous U.S.*, edited by B. C. Burchfiel, P. W. Lipman, and M. L. Zoback, Plate 2-2, Geol. Soc. of Am., Boulder, Colo., 1992.

Priestley, K., and J. Orcutt, Extremal travel time inversion of explosion seismology data from the eastern Snake River Plain, Idaho, *J. Geophys. Res., 87,* 2634-2642, 1982.

Reed, J. C., Map of the Precambrian rocks of the conterminous United States and some adjacent parts of Canada, in *The Geology of North America*, vol. C2, *Precambrian: Conterminous U.S.*, edited by J. C. Reed et al., Plate 1, Geol. Soc. of Am., Boulder, Colo., 1993.

Sheehan, A. F., G. A. Abers, C. H. Jones, and A. L. Lerner-Lam, Crustal thickness variations across the Colorado Rocky Mountains from teleseismic receiver functions, *J. Geophys. Res., 100,* 20,391-20,404, 1995.

Sheriff, S. D., and M. C. Stickney, Crustal structure of southwestern Montana and east-central Idaho: Results of a reversed seismic refraction line, *Geophys. Res. Lett., 11,* 299-302, 1984.

Sleep, N. H., Thermal effects of the formation of Atlantic continental margins by continental breakup, *Geophys. J. R. Astron. Soc., 24,* 325-350, 1971.

Smith, R. B., and M. L. Sbar, Contemporary tectonics and seismicity of the western United States with emphasis on the Intermontane seismic belt, *Geol. Soc. Am. Bull., 85,* 1205-1218, 1974.

Sparlin, M. A., L. W. Braile, and R. B. Smith, Crustal structure of the eastern Snake River Plain determined from ray trace modeling of seismic refraction data, *J. Geophys. Res., 87,* 2619-2633, 1982.

Willden, R., Seismic-refraction measurements of crustal structure between American Falls Reservoir, Idaho and Flaming Gorge Reservoir, Utah, *U.S. Geol. Surv. Prof. Pap., 525-c,* 44-50, 1965.

E. D. Humphreys and X. Peng, Department of Geological Sciences, University of Oregon, Eugene, OR 97403. (e-mail: gene@newberry.uoregon.edu)

(Received March 27, 1997; revised September 3, 1997;
accepted December 9, 1997.)